Seasonal variability of eddy kinetic energy in a global high-resolution ocean model

Jan K. Rieck,[1] Claus W. Böning,[1] Richard J. Greatbatch,[1] Markus Scheinert[1]

Corresponding author: J. K. Rieck, GEOMAR Helmholtz Centre for Ocean Research Kiel, Düsternbrooker Weg 20, 24105 Kiel, Germany. (jrieck@geomar.de)

[1]GEOMAR Helmholtz Centre for Ocean Research Kiel, Kiel, Germany.

This article has been accepted for publication and undergone full peer review but has not been through the copyediting, typesetting, pagination and proofreading process which may lead to differences between this version and the Version of Record. Please cite this article as doi: 10.1002/2015GL066152

A global ocean model with 1/12° horizontal resolution is used to assess the seasonal cycle of surface Eddy Kinetic Energy (EKE). The model reproduces the salient features of the observed mean surface EKE, including amplitude and phase of its seasonal cycle in most parts of the ocean. In all subtropical gyres of the Pacific and Atlantic, EKE peaks in summer down to a depth of ~350 m, below which the seasonal cycle is weak. Investigation of the possible driving mechanisms reveals the seasonal changes in the thermal interactions with the atmosphere to be the most likely cause of the summer maximum of EKE. The development of the seasonal thermocline in spring and summer is accompanied by stronger mesoscale variations in the horizontal temperature gradients near the surface which corresponds, by thermal wind balance, to an intensification of mesoscale velocity anomalies towards the surface.

1. Introduction

Since the advance of satellite altimetry and eddy-resolving ocean general circulation models the global view of mesoscale Eddy Kinetic Energy (EKE) and its statistics is constantly improving. Recent advances include the documentation of temporal variations in EKE which have spurred new consideration of the sources and sinks of the ocean eddy field. Using satellite altimetry *Zhai et al.* [2008] and *Scharffenberg and Stammer* [2010] obtained the striking result that surface EKE peaks in summer over most of the subtropical gyres and Western Boundary Current regions (WBCs) in both hemispheres, while it peaks in winter in the Pacific's subpolar gyre and the Labrador Sea, and has no significant seasonal cycle in most of the eastern basins and the Southern Ocean. Regional studies confirm this for the North [*Qiu*, 1999] and South Pacific [*Qiu and Chen*, 2004] subtropical gyres.

Local maxima in EKE in the vicinity of strong currents and fronts can easily be explained by baroclinic and barotropic instabilities caused by sharp gradients in velocity. Interannual changes in these instabilities, driven by either meridional shifts of the associated currents [*Hakkinen and Rhines*, 2009] or indirect effects of the wind forcing (preconditioning through Sverdrup flow [*Garnier and Schopp*, 1999], Ekman convergence and frontogenesis [*Qiu and Chen*, 2010; *Volkov and Fu*, 2011]), are thought to drive EKE variability on interannual timescales. However the generation of EKE in the interior of the midlatitude oceans is not well understood [*Xu et al.*, 2011] and several theories exist to explain EKE variability on seasonal timescales. Neither local wind forcing [*Stammer*, 1997] nor remote sources that radiate EKE into the interior of the subtropical gyres

[*Stammer et al.*, 2001] were found to satisfactorily explain the observed energy levels and spectra. It has been shown that the interior of the subtropical gyres can favor local generation of EKE by baroclinic instability, at least in regions where weak currents are present [*Beckmann et al.*, 1994; *Arbic*, 2000]. *Qiu* [1999] and *Qiu and Chen* [2004] argue that seasonally varying baroclinic instabilities between subtropical countercurrents and underlying equatorial currents are the cause for the observed seasonal cycle of surface EKE in parts of the North and South Pacific. Additionally, when considering temporal variability, dissipation of surface EKE through wind work [*Zhai and Greatbatch*, 2007] and heat fluxes [*Zhai and Greatbatch*, 2006a, b] has to be taken into account. These dissipation processes were suggested to be driving the seasonal variability of surface EKE in the Gulf Stream region, with weaker dissipation in summer [*Zhai et al.*, 2008].

Here, we report on high-resolution model simulations that shed new light onto the mechanisms of seasonal variability of surface EKE. We use a global ocean-sea ice model with 1/12° resolution to assess the spatial pattern of the annual cycle of EKE in comparison to surface altimetry. We inspect the vertical structure of the annual cycle and discuss the roles of several possible driving mechanisms with a focus on the subtropical gyres of the Atlantic and Pacific Oceans.

2. Data, Model and Methods

The observational data of geostrophic surface currents used in this study were obtained from Sea Surface Height (SSH) measurements by satellite altimetry and distributed by Archiving, Validation and Interpretation of Satellite Oceanographic Data (AVISO). It combines altimetry measurements from TOPEX/Poseidon, Jason-1, ERS-1/2 and Envisat onto a 1/4° × 1/4° grid, provided with a time step of one day, spanning the period from 01.01.1993-31.12.2012. More information on AVISO data and associated errors are found in *Le Traon et al.* [1998], *Ducet et al.* [2000] and *SSALTO/DUACS* [2011].

The model output is from a high-resolution global ocean-sea ice simulation using a model configuration (ORCA12) based on the NEMO code [*Madec et al.*, 1998], developed as part of the DRAKKAR collaboration. The various ORCA12 configurations developed in recent years [*DRAKKAR Group*, 2014] share the same global, orthogonal, curvilinear, tripolar Arakawa-C type grid with a nominal resolution of 1/12° in longitude. An ensemble of simulations from the ORCA12-suite has been used previously to examine the freshwater transport in the South Atlantic [*Deshayes et al.*, 2013] and the salt transport in the global ocean [*Tréguier et al.*, 2014]. The particular (Kiel) version of ORCA12 uses 46 vertical levels with 6 m thickness at the surface, increasing towards ∼250 m in the deep ocean and a partial-cell formulation at the bottom [cf. *Barnier et al.*, 2006]. The atmospheric forcing for the 30-year hindcast simulation (1978-2007) utilizes the bulk formulations and data products comprised in the CORE.v2 [*Griffies et al.*, 2009; *Large and Yeager*, 2009]. The model analysis focuses on the years after 1981 when the upper ocean EKE is in a quasi-equilibrium state, using 5-day mean model fields. For the calculation of $EKE = 0.5(u'^2 + v'^2)$, the zonal and meridional surface velocity fluctuations $(u', v') = (u - \bar{u}, v - \bar{v})$ represent the deviations from the annual-mean surface velocities $(\bar{u}, \bar{v})$, obtained by averaging the velocities (u, v) over each individual calendar year. Calculating (u', v') with respect to a moving average $(\bar{u}, \bar{v})$, i.e. a yearly or 3-month (removing the seasonal and interannual variability of the mean) average centered at the same time as the 5-day average, did not change amplitude and phase of the annual cycle of EKE significantly. The deviations of 5-day means from a yearly mean horizontal velocity are found to be more appropriate for seasonal EKE calculations [cf. *Penduff et al.*, 2004; *Rieck*, 2014] (Figure S1) than using the long time mean as in some previous studies [e.g. *Zhai et al.*, 2008]. EKE from surface velocities (u, v) includes a contribution from ageostrophic, e.g. Ekman, currents, which are not represented by EKE calculated from altimetry products. However, the mean, amplitude and seasonal cycle of EKE calculated from (u, v) do not differ significantly from EKE calculated from geostrophic currents from the model simulation in the subtropical gyres (cf. Figure S1). We thus use (u, v) for our analysis, as no further data processing is required.

3. Results

3.1. The annual cycle of EKE

The model realistically reproduces the spatial distribution of mean surface EKE compared to observations (Figure 1a and b) [e.g. *Zhai et al.*, 2008; *Scharffenberg and Stammer*, 2010]. All major currents are indicated by elevated EKE and the minima are located in the interior of the subtropical and subpolar gyres. Highest EKE levels are found in the vicinity of the northern hemisphere (NH) WBCs and the Agulhas Retroflection, reaching 1000-3000 cm^2/s^2. These values are comparable to the EKE values inferred from satellite altimetry [e.g. *Zhai et al.*, 2008; *Xu et al.*, 2011]. Other regions with EKE of up to 1000 cm^2/s^2 include the southern hemisphere (SH) WBCs, equatorial regions and the Antarctic Circumpolar Current (200-500 cm^2/s^2), where ORCA12, in some parts, simulates EKE somewhat higher than found in observations. In the interior subtropical gyres

EKE ranges between 5 and 50 cm^2/s^2, the SH generally shows lower values. Near current bands, e.g. subtropical countercurrents, EKE can be as high as ∼300 cm^2/s^2.

The simulated seasonal variability of EKE is compared globally to EKE derived from altimeter products by fitting a function of the form $A\cos(\omega-\phi)$ to monthly climatological EKE, with $\omega = 2\pi t/12$, $t = 1, .., 12$ (representing the months) and ϕ being the phase of the annual cycle. The distribution of the amplitude of the annual cycle of surface EKE closely follows the mean EKE (Figure 1a and b). Areas with a high mean EKE exhibit a high amplitude of the annual cycle. Amplitudes of 200 cm^2/s^2 and more can be found in some parts of the WBCs. Away from the WBCs amplitudes up to 100 cm^2/s^2 are common in the western Pacific, while in the eastern Pacific and Atlantic subtropical gyres, amplitudes are generally lower than 30 cm^2/s^2 with minima <5 cm^2/ s^2.

The phase of the annual cycle of surface EKE (the month with highest EKE) is in summer in all subtropical gyres (Figure 1c), in agreement with previous observational studies [*Zhai et al.*, 2008; *Scharffenberg and Stammer*, 2010] and analysis of AVISO data (Figure 1d). The phase from AVISO leads the simulated phase by one month in the interior subtropical gyres. This becomes especially apparent in the North and South Pacific, where more areas exhibit maximum EKE in May and October, respectively, in the obersational data.

A closer investigation of the simulated phase of the annual cycle reveals, that in the North Pacific, the Kuroshio Extension represents a transition zone between the subtropical and subpolar regimes. Maximum EKE is found in summer as far north as the axis of the Kuroshio Extension (indicated by highest EKE in Figure 1a). On the northern flank, the phase is gradually shifted towards winter. In the North Atlantic, the summer maximum of EKE extends farther north, winter maxima are restricted to regions on the continental shelf. It has to be noted though, that at higher latitudes, as well as at eastern boundaries at all extratropical latitudes, and in the Southern Ocean, the spatial distribution of the phase is heterogeneous [cf. *Zhai et al.*, 2008] with amplitudes <25 % of the mean (indicated by the hatched areas in Figure 1c), not allowing for a detailed comparison to observations (Figure 1d). A specific regional feature appearing in the model simulation is the winter maximum in EKE at, and close to, the points where the Kuroshio and Gulf Stream separate from the coasts. These are probably associated with highest baroclinic instability and thus EKE generation in winter [*Zhai et al.*, 2008]. These features could not be revealed by previous studies based on coarse resolution altimetry data [e.g. *Ducet et al.*, 2000; *Zhai et al.*, 2008] and indicate, that care has to be taken when investigating the regionally averaged seasonal cycle of EKE in WBC regions as one is prone to average over regions with substantially different variability and underlying processes.

Further analysis of seasonal variations focuses on the nature of the summer maximum of EKE in the subtropical gyres by choosing four representative regions characterized by homogeneous phase and significant amplitude of the annual cycle (Figure 1c). In the North Atlantic (NA) and South Atlantic (SA), areas in the interior (NA) or eastern subtropical basins (SA) lack a significant amplitude of the annual cycle, restricting the choice to western subtropical gyre regions. In the North Pacific (NP) and South Pacific (SP), the regions have been chosen to be comparable to the NA and SA boxes. In the NH boxes, EKE in the model is two to three times lower than EKE from observations, partly attributable to a northward shift of the WBC extensions by roughly 2°-3° in the model (Figure S2), so that while the regions chosen contain elevated EKE levels influenced by the WBC regions in the AVISO data, these areas with higher EKE are excluded from averaging in the model output. Despite this bias in the mean of the simulated seasonal cycle, surface EKE peaks in the summer months in all four subtropical gyres in the Atlantic and Pacific Oceans (Figure 2). On average, EKE is higher in the Pacific, with highest values in the NP box. The seasonal cycles, though shifted towards later in the year by ~1 month, are similar in phase and have an amplitude of ~50-60 % of the annual mean in the model, compared to 30-50 % in AVISO.

An interesting feature of the EKE variability not accessible from satellite observations is its vertical structure (Figure 3). The model simulation shows, that the seasonal cycle is markedly surface intensified with values of up to ~50 cm^2/s^2 (~25 cm^2/s^2) at the surface in the NP and SP boxes (NA and SA boxes), decreasing rapidly within the upper 150-200 m, while the phase of the seasonal cycle is similar over this depth range (cf. Figure 4). As at the surface, EKE in the upper 350 m is about two to three times higher in the Pacific boxes, compared to the Atlantic boxes (Figure 4). Strong variations on a seasonal time scale are only observed in the upper 100 m of the water column; below ~350 m EKE is ~10 cm^2/s^2 in all four regions (Figure 4) and the amplitude of the seasonal cycle is <5 cm^2/s^2.

3.2. Possible mechanisms

Several possible mechanisms have been proposed to explain the observed seasonal variations of surface intensified EKE in the interior subtropical gyres. In the following, we use the model to test these hypotheses.

First, EKE together with its seasonal cycle could be advected or radiated from regions with strong currents into less energetic regions [*Pedlosky*, 1977; *Chester et al.*, 1994; *Xu et al.*, 2014]. Although advection of EKE cannot be ruled out in general, it is clearly not the cause for the observed seasonal variations. In particular, there is no phase shift observed from regions of higher EKE towards the interior gyres, as is the case e.g. in the Indian Ocean's Leeuwin Current [*Scharffenberg and Stammer*, 2010], the California Current and off the Peruvian coast (Figure 1c), where EKE is produced near the continents and then propagates towards the interior, shifting the phase of the seasonal cycle towards later in the year ($\sim$0.5-1 months/°longitude) in agreement with eddy propagation speeds of $\sim$3-5 km/day [e.g. *Fu*, 2009].

Next, wind work could damp the EKE at the surface, imprinting the seasonal variations of the wind field onto the EKE [*Zhai and Greatbatch*, 2007]. The monthly mean climatology of wind stress amplitude τ from the model is depicted in Figure 2. The wind stress amplitude shows significantly different behavior in the different gyres. While the SA box has a clear winter maximum (>0.05 N/m^2 compared to 0.03 N/m^2 in summer), the NA box shows a winter and a summer maximum with comparable amplitudes (0.06 N/m^2). The NP box wind stress amplitude (in the range 0.04-0.08 N/m^2) does not exhibit any clear seasonal cycle and the SP box has a weak fall minimum (0.04 N/m^2) but no clear maximum (0.05-0.06 N/m^2). These findings suggest the wind stress to be of minor importance for EKE dissipation in the subtropical gyres, compared to the role it could play in the WBC regimes [*Zhai et al.*, 2008].

A third hypothesis proposed to induce a seasonal cycle of surface EKE, is through dissipation of Sea Surface Temperature (SST) anomalies due to surface heat fluxes [*Zhai and Greatbatch*, 2006a, b]. This is found to be consistent with the model simulation, where in winter, downward heat flux anomalies in the mesoscale are larger for the same change in SST than in summer (-58.1 W/m^2/°C in DJF, -40.9 W/m^2/°C in JJA, as calculated for part of the western NA subtropical gyre). This means that the damping due to surface heat flux applied to the depth of the seasonal thermocline is less in summer than it is in winter.

However, another and probably a more important aspect of the seasonality in surface heat fluxes and the resulting seasonal thermocline is the associated intensification of mesoscale currents towards the surface. A conspicuous aspect of the model results is the small vertical penetration of the annual signal: EKE values below ~350 m depth are almost constant throughout the year (Figure 3). Thermal wind balance then requires horizontal mesoscale temperature gradients to support the vertical shear of the mesoscale velocities associated with the seasonal maximum of EKE in summer. Figure 4 shows $T_{grad} = [(\partial T/\partial x)^2 + (\partial T/\partial y)^2]^{1/2}$, where T are high-pass filtered temperature anomalies (wavelengths $<$ ~450 km). In winter, when the Mixed Layer (ML) is deep, T_{grad} is small (4-8×10^{-6} °C/m) and the velocities are only weakly sheared towards the surface. This reduction in T_{grad} and the associated velocities is easily explained by large scale surface heat loss, inducing a homogenization and deepening of the ML. Contrastingly, when the ML shoals in spring, T_{grad} associated with the seasonal thermocline increases to 8-14$\times10^{-6}$ °C/m. The reasons behind this reappearance of strong T_{grad}, in contrast to the erosion in fall and winter, is less clear and will be further discussed in the following section. Nevertheless, these higher gradients require the mesoscale currents from below 350 m to strongly intensify towards the surface, resulting in a summer maximum of EKE at the surface.

4. Summary and Discussion

The ORCA12 model was found to reproduce the observed annual cycle of surface EKE on a global and regional scale, especially in our regions of interest, the Atlantic and Pacific subtropical gyres. Surface EKE, vertical and meridional EKE profiles, and seasonal cycles were also compared to two other models with lower (1/4°) (Figure 3, S2 and S3) and higher (1/20°) (Figure S3) resolution (see *Behrens* [2013] for details on the model configurations). No qualitative differences to the results from the 1/12° model are observed, indicating robustness of the findings, not only at the surface, where a comparison to observations on a global scale is possible, but also in the sub-surface subtropical ocean, where only a very limited number of mooring observations have been investigated for seasonal variations [*Wunsch*, 1997].

The model simulation aids in the explanation of the observed seasonal variability and provides a 3-d perspective of the phenomenon not available from observations on a global scale. A striking feature is the broad summer maximum in EKE across both hemispheres found in both, the model and the observations.

Advection of EKE from regions with high EKE towards the interior ocean basins can be ruled out as a source for the observed seasonal variability of surface EKE, as there is no phase shift in the annual cycle to support such a mechanism. Likewise, the wind stress and associated dissipation of EKE is only of minor importance to the subtropical gyres, as they do not have a common observed wind stress cycle, despite having a similar seasonal variability in EKE.

The remaining external forcing to contribute to the seasonal cycle of EKE in the subtropical gyres are thermal interactions with the atmosphere. In a direct way, surface heat fluxes exert a damping of mesoscale anomalies [*Zhai and Greatbatch*, 2006b]. We have seen that the net damping over the depth of the seasonal thermocline is weaker in summer than in winter. The ML is deeper and the mesoscale surface heat flux anomalies for the same change in SST are stronger in winter, leading to an enhanced damping, which is reduced during summer when there is also a strong decoupling of the deeper layers through the seasonal thermocline from the surface due to the strong stratification.

A key new aspect revealed by the model simulation concerns the vertical structure of the EKE variation. The surface-trapped nature of the seasonal cycle of EKE implies an enhanced vertical shear of mesoscale velocity variations in summer, corresponding to stronger horizontal mesoscale temperature gradients because of thermal wind balance (cf. Figure 4). While the erosion of these gradients in fall and early winter is easy to understand as a consequence of large scale cooling due to surface heat loss, their regeneration in spring is less clear. One possibility is that the continuous, year round production of EKE in combination with the surface heat input generates these mesoscale temperature gradients without the need to invoke a seasonal cycle in EKE production from baroclinic instability. Another possibility is a seasonally varying production of EKE through baroclinic instability in the top 200-300 m [e.g. *Beckmann et al.*, 1994] as proposed by *Qiu* [1999] and *Qiu and Chen* [2004] for parts of the Pacific subtropical gyres. Since this depends on the presence of vertically sheared currents over the depth range of the seasonal thermocline that are present in the Pacific but are less pronounced in the Atlantic subtropical gyres, this might help explain the larger amplitude of the seasonal cycle of the EKE in the NP and SP boxes compared to the NA and SA boxes.

The relative importance of the influence from the different mechanisms on the seasonal cycle of surface EKE cannot be determined by this analysis. An interesting point in this regard is that the seasonal cycle of upper ocean EKE is consistent through simulations with various resolutions. Various previous studies suggested the importance of submesoscale EKE with scales on the order $O(10$ km$)$ in modulating the seasonal cycle of EKE [*Hristova et al.*, 2014; *Qiu et al.*, 2014] and maintaining mesoscale EKE levels [*Sasaki et al.*, 2014]. However, since the submesoscale on the order $O(10$ km$)$ is not resolved in models with $O(1/4°)$ meshes, the mechanisms involving these scales can only be of minor importance to the seasonal cycle of mesoscale surface EKE, possibly adding small modulations in higher-resolution models and the real ocean.

Acknowledgments. This study is a contribution to the cooperative project RACE (Regional Atlantic Circulation and Global Change, grant 03F0651B), funded by the German Federal Ministry for Education and Research (BMBF) and the Cluster of Excellence "The Future Ocean", funded by the Deutsche Forschungsgemeinschaft (DFG). The model system has been developed by the ocean modelling group at GEOMAR in the framework of the DRAKKAR collaboration. The authors thank Erik Behrens for providing output from the ORCA025 and VIKING20 simulations, which were performed at the North-German Supercomputing Alliance (HLRN). The ORCA12 simulation was performed at the German Climate Computing Center (DKRZ). The authors further thank three anonymous reviewers for their helpful comments on earlier versions of this manuscript. Data shown in this paper are available by email from data-tm@geomar.de.

References

Arbic, B. K. (2000), Generation of mid-ocean eddies: The local baroclinic instability hypothesis, Ph.D. thesis, Massachusetts Institute of Technology and Woods Hole Oceanographic Institution, Massachusetts.

Barnier, B., G. Madec, T. Penduff, J.-M. Molines, A.-M. Tréguier, J. Le Sommer, A. Beckmann, A. Biastoch, C. Böning, J. Dengg, C. Derval, E. Durand, S. Gulev, E. Remy, C. Talandier, S. Theetten, M. Maltrud, J. McClean, and B. De Cuevas (2006), Impact of partial steps and momentum advection schemes in a global ocean circulation model ata eddy permitting resolution, *Ocean Dyn.*, *56*(5-6), 543–567.

Beckmann, A., C. W. Böning, B. Brügge, and D. Stammer (1994), On the generation and role of eddy variability in the central North Atlantic Ocean, *J. Geophys. Res.*, *99*, C10.

Behrens, E. (2013), The oceanic response to Greenland melting: The effect of increasing model resolution, Ph.D. thesis, Christian-Albrechts-Universität zu Kiel, Kiel.

Chester, D., P. Malanotte-Rizzoli, J. Lynch, and C. Wunsch (1994), The eddy radiation field of the Gulf Stream as measured by ocean acoustic tomography, *Geophys. Res. Lett.*, *21*(3), 181–184.

Deshayes, J., A.-M. Tréguier, B. Barnier, A. Lecointre, J. Le Sommer, J.-M. Molines, T. Penduff, R. Bourdallé-Badie, Y. Drillet, G. Garric, R. Benshila, G. Madec, A. Biastoch, C. W. Böning, M. Scheinert, A. C. Coward, and J. J.-M. Hirschi (2013), Oceanic hindcast simulations at high resolution suggest that the Atlantic MOC is bistable, *Geophys. Res. Lett.*, *40*, 1–5, doi:10.1002/grl.50534.

DRAKKAR Group (2014), DRAKKAR: developing high resolution ocean components for European Earth system models, *Clivar Exchanges No. 65*, *19*(2), 18–20.

Ducet, N., P. Y. Le Traon, and G. Reverdin (2000), Global high-resolution mapping of ocean circulation from TOPEX/Poseidon and ERS-1 and -2, *J. Geophys. Res. Oceans*, *105*, 19,477–19,498.

Fu, L.-L. (2009), Pattern and velocity of propagation of the global ocean eddy variability, *J. Geophys. Res.*, *114*, C11017, doi:10.1029/2009JC005349.

Garnier, V., and R. Schopp (1999), Wind influence on the mesoscale activity along the Gulf Stream and the North Atlantic currents, *J. Geophys. Res.*, *104*, C8, 18087–18110, doi:10.1029/1999JC900070.

Griffies, S. M., A. Biastoch, C. Böning, F. Bryan, G. Danabasoglu, E. P. Chassignet, M. H. England, R. Gerdes, H. Haak, R. W. Hallberg, W. Hazeleger, J. Jungclaus, W. G. Large, G. Madec, A. Pirani, B. L. Samuels, M. Scheinert, A. Sen Gupta, C. A. Severijns, H. L. Simmons, A. M. Tréguier, M. Winton, S. Yeager, and J. Yin (2009), Coordinated ocean-ice reference experiments (COREs), *Ocean Model.*, *26*, 1–46.

Hakkinen, S., and P. B. Rhines (2009), Shifting surface currents in the northern North Atlantic Ocean, *J. Geophys. Res.*, *114*, C04005, doi:10.1029/2008JC004883

Hristova, H. G., W. S. Kessler, J. C. McWilliams, and M. J. Molemaker (2014), Mesoscale variability and its seasonality in the Solomon and Coral Seas, *J. Geophys. Res. Oceans*, *119*, 4669–4687, doi:10.1002/2013JC009741.

Large, W. G., and S. G. Yeager (2009), The global climatology of an interannually varying air-sea flux data set, *Clim. Dyn.*, *33*, 341–364, doi:10.1007/s00382-008-0441-3.

Le Traon, P. Y., F. Nadal, and N. Ducet (1998), An improved mapping method of multi-satellite altimeter data, *J. Atmos. Ocean. Technol.*, *15*, 522–534.

Madec, G., P. Delecluse, M. Imbard, and C. Lévy (1998), OPA 8.1 Ocean General Circulation Model reference manual, *Notes du Pôle de modélisation*, Institut Pierre-Simon Laplace (IPSL).

Pedlosky, J. (1977), On the radiation of meso-scale energy in the mid-ocean, *Deep-Sea Res.*, *24*, 591–600.

Penduff, T., B. Barnier, W. K. Dewar, and J. J. O'Brien (2004), Dynamical responses of the oceanic eddy field to the North Atlantic Oscillation: A model-data comparison, *J. Phys. Oceanogr.*, *34*, 2615–2629.

Qiu, B. (1999), Seasonal eddy field modulation of the North Pacific Subtropical Countercurrent: TOPEX/Poseidon observations and theory, *J. Phys. Oceanogr.*, *29*, 2471–2486.

Qiu, B., and S. Chen (2004), Seasonal modulations in the eddy field of the South Pacific Ocean, *J. Phys. Oceanogr.*, *34*, 1515–1527.

Qiu, B., and S. Chen (2010), Interannual variability of the North Pacific Subtropical Countercurrent and its associated mesoscale eddy field, *J. Phys. Oceanogr.*, *40*, 213–225, doi:10.1175/2009JPO4285.1.

Qiu, B., S. Chen, P. Klein, H. Sasaki, and Y. Sasai (2014), Seasonal mesoscale and submesoscale eddy variability along the North Pacific Subtropical Countercurrent, *J. Phys. Oceanogr.*, *44*, 3079–3098, doi:10.1175/JPO-D-14-0071.1.

Rieck, J. K. (2014), Temporal variability of oceanic eddy kinetic energy: A high resolution model analysis, M.Sc. thesis, Christian-Albrechts-Universität zu Kiel, Kiel.

Sasaki, H., P. Klein, B. Qiu, and Y. Sasai (2014), Impact of oceanic-scale interactions on the seasonal modulation of ocean dynamics by the atmosphere, *Nat. Commun.*, *5:5636*, doi:10.1038/ncomms6636.

Scharffenberg, M. G., and D. Stammer (2010), Seasonal variations of the large-scale geostrophic flow field and eddy kinetic energy inferred from the TOPEX/Poseidon and Jason-1 tandem mission data, *J. Geophys. Res.*, *115*, C02008, doi: 10.1029/2008JC005242.

SSALTO/DUACS (2011), User Handbook: (M)SLA and (M)ADT near-real time and delayed time products, *Cls_dos_nt_06-034 issue 2.5*.

Stammer, D. (1997), Global characteristics of ocean variability estimated from regional TOPEX/POSEIDON altimeter measurements, *J. Phys. Oceanogr.*, *27*, 1743–1769.

Stammer, D., C. Böning, and C. Dietrich (2001), The role of variable wind forcing in generating eddy energy in the North Atlantic, *Prog. Oceanogr.*, *48*, 289–311.

Tréguier, A. M., J. Deshayes, J. Le Sommer, C. Lique, G. Madec, T. Penduff, J.-M. Molines, B. Barnier, R. Bourdallé-Badie, and C. Talandier (2014), Meridional transport of salt in the global ocean from an eddy-resolving model, *Ocean Sci.*, *10*, 243–255, doi: 10.5194/os-10-243-2014.

Volkov, D. L., and L.-L. Fu (2011), Interannual variability of the Azores Current strength and eddy energy in relation to atmospheric forcing, *J. Geophys. Res. Lett.*, *116*, C11011, doi:10.1029/2011JC007271.

Wunsch, C. (1997), The vertical partition of oceanic horizontal kinetic energy, *J. Phys. Oceanogr.*, *27*, 1770–1794.

Xu, C., X.-D. Shang, and R. X. Huang (2011), Estimate of eddy energy generation/dissipation rate in the world ocean from altimetry data, *Ocean Dyn.*, *61*, 525–541, doi:10.1007/s10236-011-0377-8.

Xu, C., X.-D. Shang, and R. X. Huang (2014), Horizontal eddy energy flux in the world oceans diagnosed from altimetry data, *Sci. Rep.*, *4*, 5316, doi:10.1038/srep05316.

Zhai, X., and R. J. Greatbatch (2006a), Inferring the eddy-induced diffusivity for heat in the surface mixed layer using satellite data, *Geophys. Res. Lett.*, *33*, L24607, doi: 10.1029/2006GL027875.

Zhai, X., and R. J. Greatbatch (2006b), Surface eddy diffusivity for heat in a model of the northwest Atlantic Ocean, *Geophys. Res. Lett.*, *33*, L24611, doi:10.1029/2006GL028712.

Zhai, X., and R. J. Greatbatch (2007), Wind work in a model of the northwest Atlantic Ocean, *Geophys. Res. Lett.*, *34*, L04606, doi:10.1029/2006GL028907.

Zhai, X., R. J. Greatbatch, and J.-D. Kohlmann (2008), On the seasonal variability of eddy kinetic energy in the Gulf Stream region, *Geophys. Res. Lett.*, *35*, L24609, doi: 10.1029/2008GL036412.

Figure 1. a), b): Amplitude of the annual cycle of surface EKE (colors, note the non-linear scale) and mean surface EKE (contours at 20, 50, 200 and 500 cm^2/s^2) for a) ORCA12 and b) AVISO. c), d): Phase of the annual cycle of surface EKE (month with highest EKE) for c) ORCA12 and d) AVISO. Both the amplitude and phase are from a fitted annual cycle as described in the text. Regions used for more detailed investigations are indicated by green boxes (NP: North Pacific; SP: South Pacific; NA: North Atlantic; SA: South Atlantic). In c) and d), regions where the amplitude of the annual cycle is $<$25 % of the mean are masked by hatches.

Figure 2. Monthly climatological EKE from ORCA12 (solid black line; cm^2/s^2), EKE from satellite altimetry (dashed black line; cm^2/s^2) and wind stress amplitude τ (dotted red line; N/m^2) for the four regions shown in Figure 1c and d. NP (a); 20°N-30°N; 160°E-175°W), SP (c); 25°S-35°S, 150°W-175°W), NA (b); 20°N-30°N, 45°W-65°W) and SA (d); 25°S-35°S, 20°W-40°W). Note the differently scaled y-axis in a).

Figure 3. Amplitude of the seasonal cycle of EKE plotted against depth for a), the 1/12° model (ORCA12) and b), the 1/4° model (ORCA025) averaged over the NP (solid line), SP (dashed line), NA (dash-dotted line) and SA (dotted line) boxes.

Figure 4. Monthly climatological square root of the variance of mesoscale, horizontal temperature gradients (T_{grad} C°/1000 km) plotted against depth in colors for the four regions shown in Figure 1c, NP (a), SP (c), NA (b) and SA (d). Gray contours depict monthly climatological EKE, units are cm^2/s^2. Contour levels are (20, 40, 60, 80, 100) and (10, 20, 30, 40, 50) for a), c) and b), d) respectively, every other contour is labelled. The white line indicates the mean Mixed Layer Depth. Note the different color scales for the left and right panels.

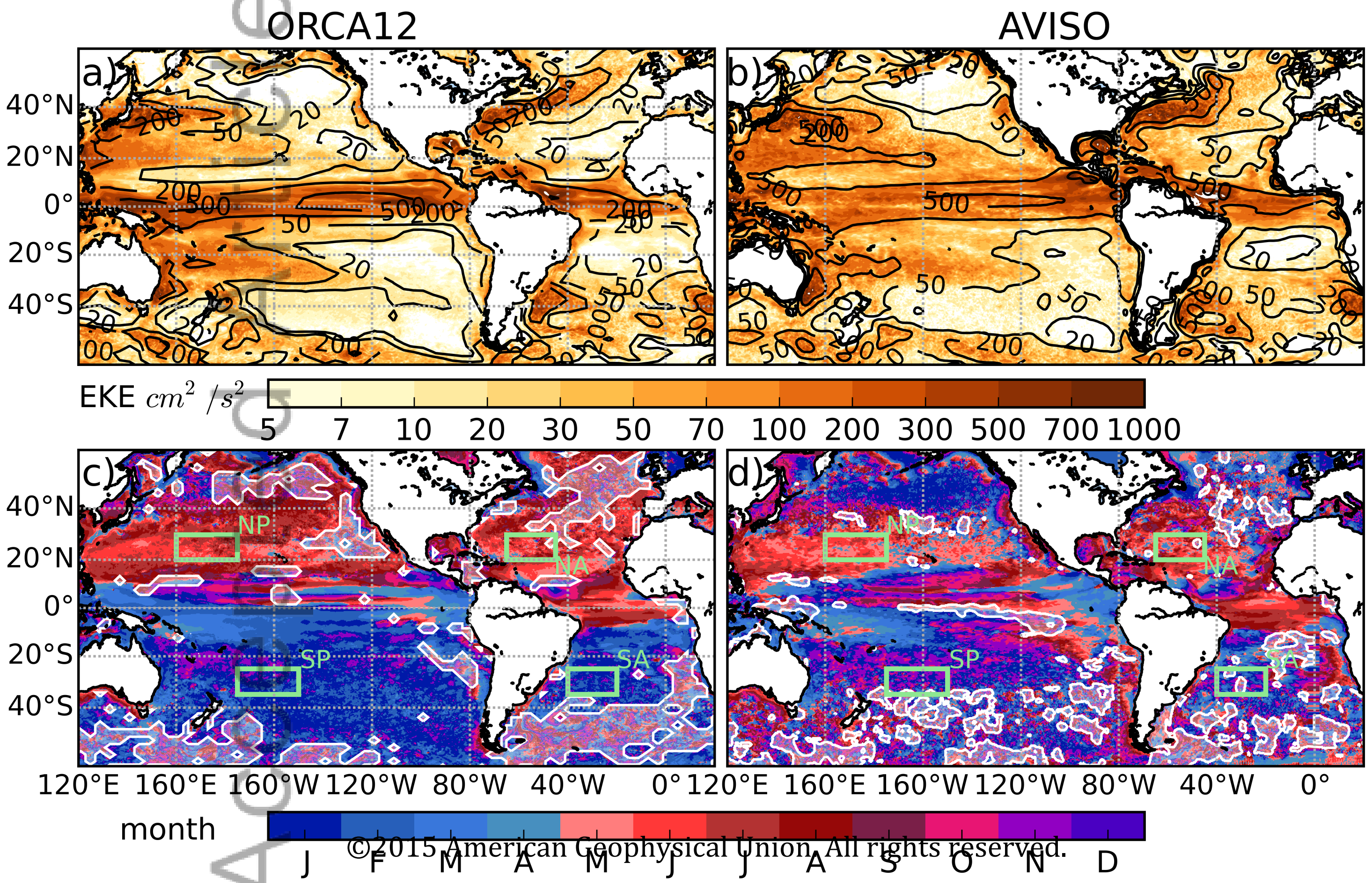
ORCA12
AVISO
a)
b)
c)
d)
EKE cm^2/s^2
5 7 10 20 30 50 70 100 200 300 500 700 1000
NP
NA
SP
SA
40°N
20°N
0°
20°S
40°S
120°E 160°E 160°W 120°W 80°W 40°W 0°
month
J F M A M J J A S O N D

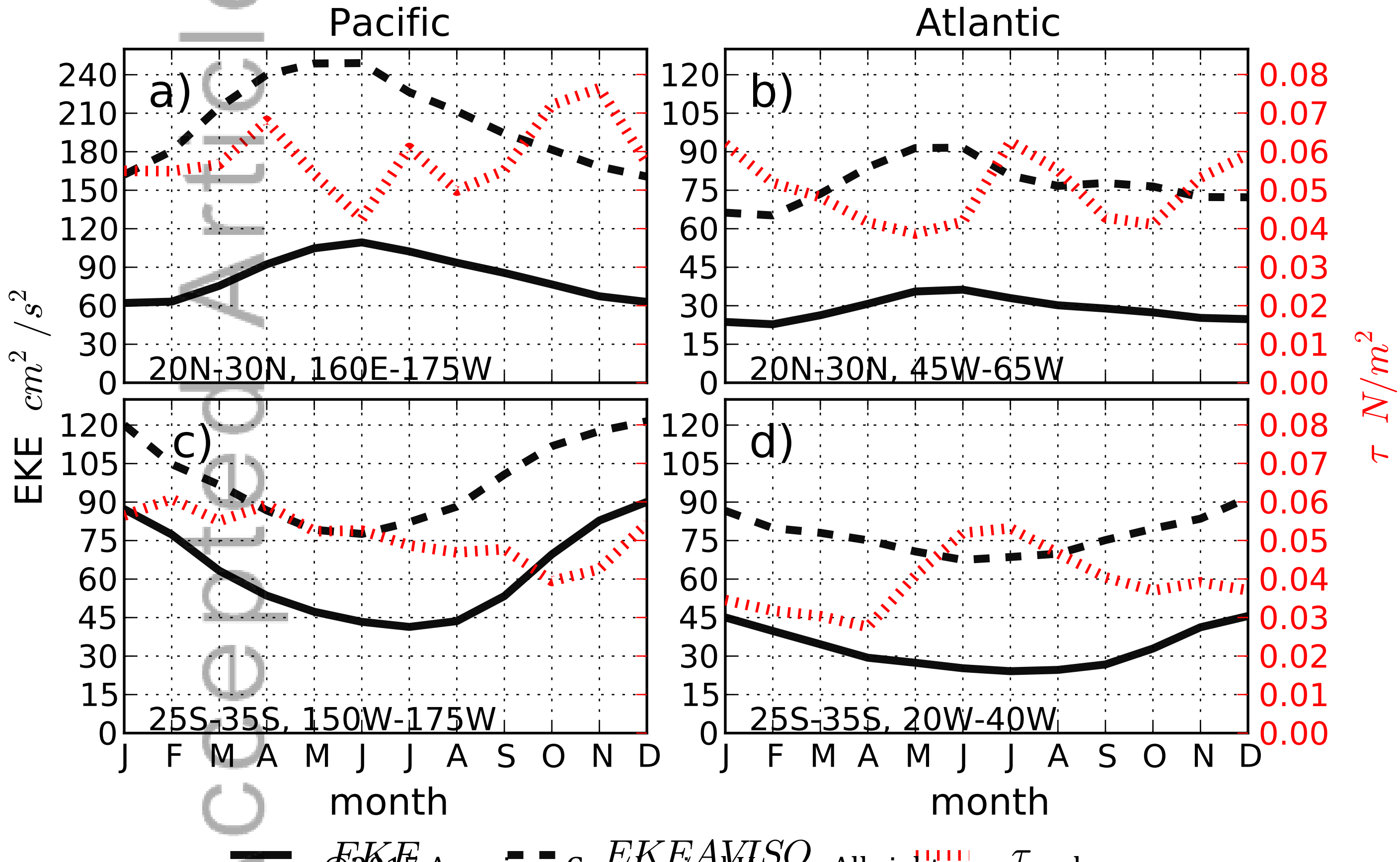

Pacific
Atlantic
a)
b)
c)
d)
20N-30N, 160E-175W
20N-30N, 45W-65W
25S-35S, 150W-175W
25S-35S, 20W-40W
EKE cm^2/s^2
τ N/m^2
month
month
J F M A M J J A S O N D
EKE
EKEAVISO
τ

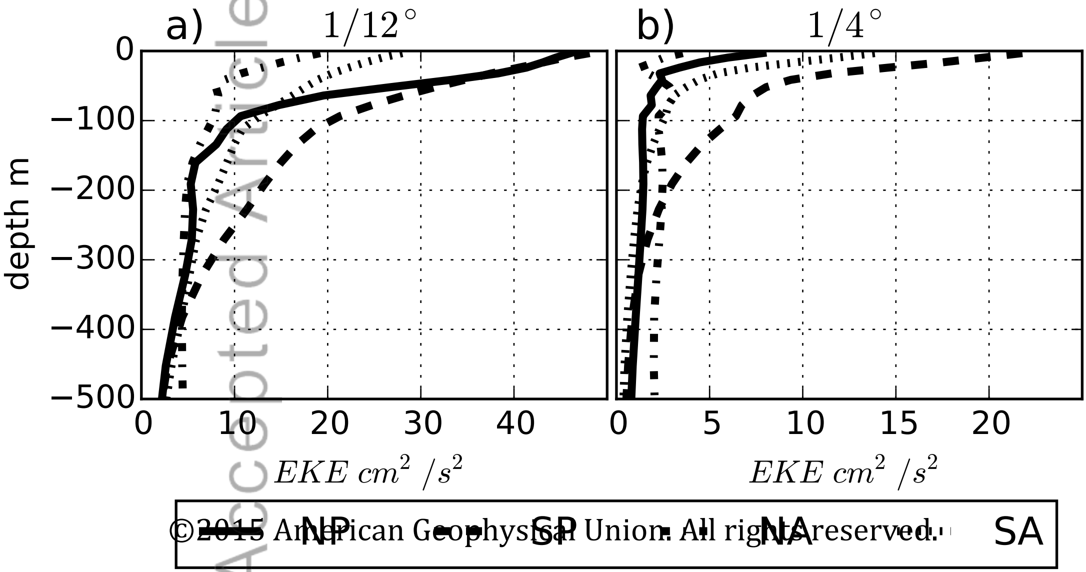

a)
1/12°
b)
1/4°
depth m
EKE cm^2/s^2
EKE cm^2/s^2
NP
SP
NA
SA

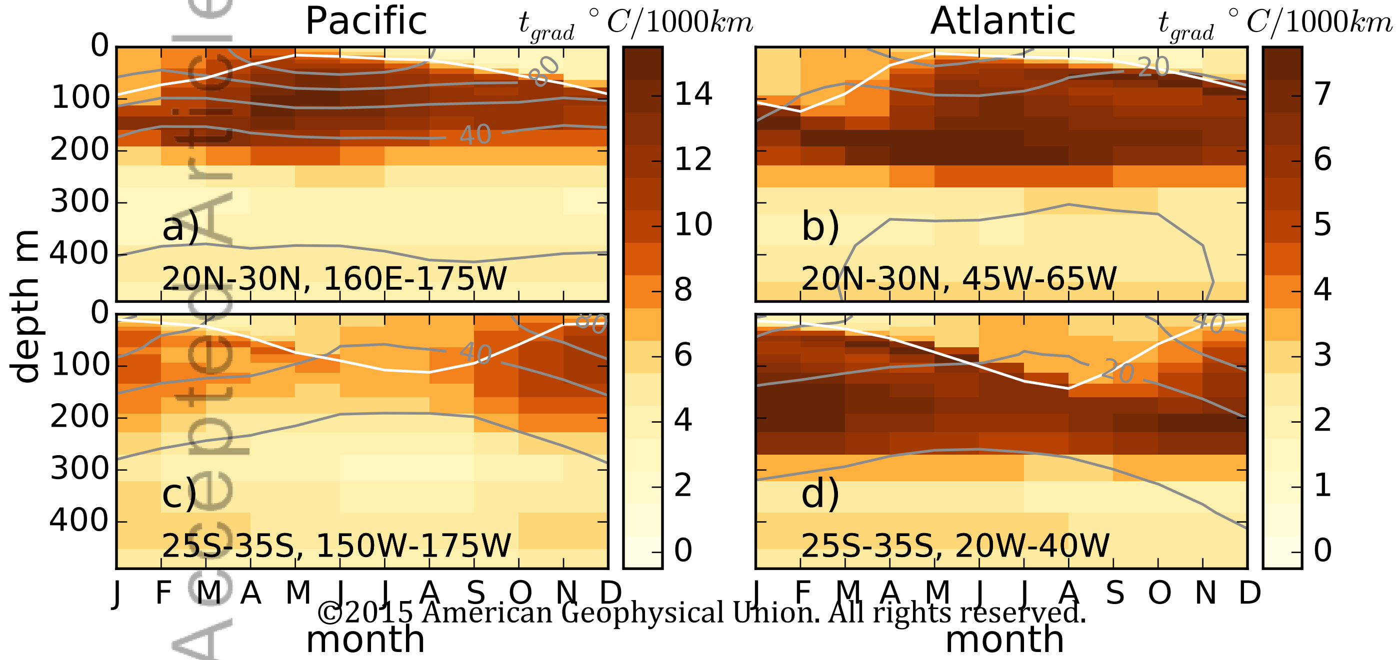

Pacific
Atlantic
t_{grad} °C/1000km
depth m
a)
20N-30N, 160E-175W
b)
20N-30N, 45W-65W
c)
25S-35S, 150W-175W
d)
25S-35S, 20W-40W
month
J F M A M J J A S O N D